Fluorescence photobleaching recovery spectroscopy in a dye doped nematic liquid crystal

P. Etchegoin
Centro Atómico Bariloche and Instituto Balseiro, Comisión Nacional de Energía Atómica and Universidad Nacional de Cuyo, 8400 San Carlos de Bariloche, Río Negro, Argentina
(Received 25 August 1998)

The process of dye diffusion through a nematic liquid crystal (LC) host is studied by fluorescence photobleaching recovery spectroscopy and digital imaging. The effects of temperature and anisotropy on the diffusion of photobleached dye molecules within a planar aligned LC cell are explicitly shown. Furthermore, the possibility of utilizing Raman rather than fluorescence imaging for the study of diffusion in binary mixtures of fluorescence-free nematoges is suggested. [S1063-651X(99)10902-4]

PACS number(s): 61.30.Gd, 87.64.Ni, 78.20.Fm, 32.80.Lg

I. INTRODUCTION AND OVERVIEW

The *in situ* study of the diffusion dynamics of fluorescently tagged proteins or dextrants within cells or biologically relevant fluids is a customary practice in the field of biophotonics [1,2]. Normally, dyes which bind to specific macromolecules or proteins are employed as tracers to follow the particular dynamics of the latter. The dyes can be resonantly pumped by an external laser which is usually focused by a microscope objective. The fluorescence emitted by the tagged molecules can be collected by the same objective, to be subsequently filtered and detected. If photobleaching of the dyes takes place within the focal region of the objective, a decay of the fluorescence signal is observed in the early stages of laser illumination. The decay time produced by photobleaching depends on the input power, specific laser wavelength, and peculiarities of the absorption spectrum of the dyes. On the other hand, if the laser is turned off for a given period of time, a recovery of the fluorescence signal can be observed when the laser illumination is reinstated, for diffusion of new molecules takes place from the neighboring regions into the focal volume of the laser spot. In this manner, the diffusion process of the tagged molecules themselves can be studied. Diffusion of biomolecules is, in fact, one of the most basic an important mechanisms in cell biology [3], and can be microscopically studied in this manner. The term *fluorescence photobleaching recovery spectroscopy* (FPRS) has been coined as a general description of this method. The technique has different variations according to the details of the specific experiment. In particular, the geometrical aspects of the illuminating optics and the imaging method to monitor the fluorescence emission (normal, confocal, etc.) determine the type of experiment under consideration. Very recently, the usage of two-photon scanning microscopy in addition to FPRS has been proposed [4] as a method for creating a flat, almost two-dimensional, distribution of photobleached molecules, allowing a better control of the initial conditions before diffusion takes place.

Liquid crystals (LC's) are complex fluids with intrinsic long range orientational order and intricate hydrodynamic properties [5]. Dye molecules can be diluted within a LC to take advantage, in this manner, of the intrinsic molecular order of the liquid crystalline phases, and become oriented along particular directions. The induced macroscopic order of the dyes was called *guest-host interaction* by Heilmeier, Castellano, and Zanoni, who observed it for the first time [6]. Since the absorption of the dyes is normally very anisotropic, dye doped LC's are ideal systems where dichroism can be controlled by external parameters like temperature and magnetic or electric fields. Furthermore, the addition of dyes to nematic liquid crystals has been shown to be the source of several very interesting and complex nonlinear optical properties. In particular, the observation of enhanced optical torques [7,8], unusual reorientation dynamics upon ultrashort laser illumination [9], and permanent holographic recording of patterns [10] are a few incomplete examples of the rich optical properties of these systems. From the viewpoint of applications, dye doped LC's seem to be promising substances for electro-optic devices with enhanced contrast ratios in the visible [11].

The diffusion process of dyes in LC's has heretofore been poorly studied. In this paper, we shall concentrate on the study of dye diffusion through both oriented and unoriented nematic liquid crystal hosts. In particular, the application of FPRS, the effect of temperature, and a direct view into the diffusion process by means of digital imaging of the fluorescence emission will be demonstrated. Dye diffusion within an ordered nematic LC cell takes place in an anisotropic manner, which ensures the long term preservation of the dichroism. A direct view into the diffusion process of photobleached dye molecules will be shown by virtue of a two-beam FPRS technique. The interplay between photobleaching and diffusion will be explicitly shown, as well as the effect of temperature on a planar oriented LC cell where dye molecules are locally photobleached. Moreover, we show that Raman rather than fluorescence signals could be used to study the interdiffusion of transparent substances like binary mixtures of nematogens, where intrinsic fluorescence cannot be used.

The paper is organized as follows: Section II presents the experimental setup for the forthcoming experiments, the sample preparation, a description of the interpretation of the data, and the experimental findings. The necessary theoretical background is also supplied in Sec. II, whenever it is relevant for the interpretation of the data. Finally, in Sec. III, a brief discussion is presented and a few conclusions are bestowed.

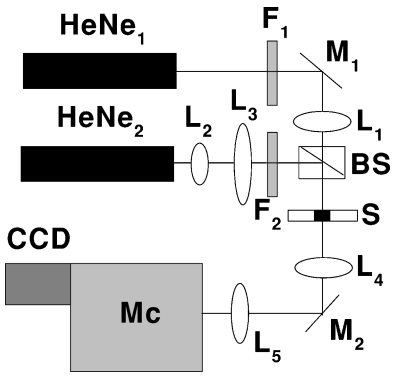

FIG. 1. Experimental setup used for FPRS or digital imaging of the diffusion process in a dye doped LC. L_i: lenses; M_i: mirrors; F_i: filters; BS: beam splitter; S: sample, hot stage; Mc: monochromator; CCD: detector. The sample (S) can be shone by either one laser beam coming from $HeNe_1$ and focused by L_1 or two lasers if the expanded beam (by the telescope L_2-L_3) of $HeNe_2$ is also combined with the former at BS. Mc can be either a double subtractive monochromator coupled to a 2D CCD array for digital imaging, or a triple subtractive monochromator coupled to a photomultiplier tube (PMT) for fluorescence measurements. See text for further details.

II. EXPERIMENTS

A. Experimental setup

All the experiments reported in this paper made use of the experimental setup shown in Fig. 1 and slight variations of it. In the experiments we shall describe subsequently, the sample (S) is either a hot stage for LC cells, where transmission experiments can be performed and temperature can be controlled in the range 20–150 °C, or a small quartz capillar where dye diffusion through an unoriented LC sample will be studied at a fixed temperature. The sample can be illuminated either by one or two crossed polarized He-Ne lasers, $HeNe_1$ (17 mW) and $HeNe_2$ (5 mW), which are focused and expanded, respectively. $HeNe_1$ is attenuated by F_1, and focused onto the sample by L_1 through the beam splitter (BS). The beam diameter of the spot on the sample produced by $HeNe_1$ can be controlled by varying the distance from L_1 to S. $HeNe_2$ is expanded by the telescope L_2–L_3, attenuated by F_2, and combined with the beam from $HeNe_1$ at the BS, where it is directed toward the sample. L_4 and L_5 form an image of the sample onto the monochromator (Mc) entrance. The monochromator is used in two different modes depending on the experiment. Mc is, in some of the reported experiments, a double subtractive monochromator with an intermediate slit acting as a spectral filter. The output of the second stage is, in this manner, the same image formed on the entrance slit but filtered at a given wavelength, with a bandwidth that depends on the aperture of the intermediate slit. The image is sent onto a cooled charge-coupled-device (CCD) array, where it can be digitally recorded. Conversely, Mc is used in a triple subtractive configuration, i.e., the output of the double subtractive stage is sent to a third grating where the light is dispersed and analyzed either by a photomultiplier tube (PMT), for fluorescence measurements, or a CCD array, for Raman signals. All these configurations are allowed by a Jobin-Yvon T64000 triple spectrometer. The different applications of this setup with one or two beams being shone onto the sample will be further clarified in Sec. II B.

The sample was made from the nematic liquid crystal mixture E_7 (Merck) (nematic range ~ -10–$63\,^{\circ}\mathrm{C}$). The sample preparation followed that of Ref. [8]. We used a planar aligned LC cell with a thickness of 100 μm achieved by a mica spacer and a dye concentration of 10^{-3} mg/ml. The dye was 3,3'-diethylthiadicarbocyanine iodide (DTDCI), which has its absorption and fluorescence maxima at ~ 655 and 695 nm, respectively [8]. For the diffusion experiments through an unoriented LC sample within a quartz capillar, we used a mixture of E_7, and DTDCI with a concentration of 10^{-2} mg/ml.

B. Modeling overview

We start by gathering the necessary information based on simple models to discuss the experimental findings and the coexistence of photobleaching and dye diffusion in a planar aligned dye doped nematic LC cell. Exactly as in Ref. [8] we shall refer to two possible configurations to monitor the fluorescence emission of the dyes. The incoming laser light of $HeNe_1$, $\vec{E}_L^1$, is polarized along the vertical direction, and an analyzer is placed before the entrance slit of the monochromator parallel to $\vec{E}_L^1$. The LC cell in between will be oriented with the director $\vec{n}$ either $\parallel$ or $\perp$ to $\vec{E}_L^1$. We shall refer to these two configurations as *parallel* or *perpendicular* excitation, and their fluorescence signals will be represented by $I_\parallel$ and $I_\perp$, respectively. After Ref. [8], photobleaching of the dyes will produce two characteristic decay times of the fluorescence emission for the two aforementioned excitation conditions; to wit, $\tau_\parallel \propto (I_0^2 \langle \cos^4(\Theta) \rangle_T)^{-1}$ and $\tau_\perp \propto (I_0^2 \langle \sin^4(\Theta) \rangle_T)^{-1}$, where Θ is the angle between the principal axis of a given LC molecule and the direction of $\vec{E}_L^1$, $I_0 = (E_L^1)^2$, and $\langle\ \rangle_T$ denotes a thermal average which takes into account the spread of orientations around $\vec{n}$ according to the order parameter in the nematic state at a given temperature T. If diffusion of the dyes within the LC did not exist, the fluorescence signals $I_{\parallel,\perp}$ would decay with time constants $\tau_{\parallel,\perp}$, and approach a zero limiting value when the dye concentration within the laser spot is fully exhausted. Conversely, if diffusion were extremely fast compared to the characteristic times $\tau_{\parallel,\perp}$, the fluorescence signals $I_{\parallel,\perp}$ would never be seen to decay. The diffusion process has a characteristic response τ_D related to the time it takes for a uniform dye distribution to recover from a small perturbation in the local concentration. In general, the observed decay time in $I_{\parallel,\perp}$ will depend on both $\tau_{\parallel,\perp}$ and τ_D. Since $\tau_{\parallel,\perp}$ depends on I_0, it will be in most cases possible to go from a regime where $\tau_{\parallel,\perp} \ll$ or $\gg \tau_D$ to a situation where $\tau_{\parallel,\perp} \sim \tau_D$. The simplest model that takes into account the time evolution of the fluorescence emission is of the form

$$\frac{dI_{\parallel,\perp}(t)}{dt} = -\frac{I_{\parallel,\perp}(t)}{\tau_{\parallel,\perp}} - \left(\frac{I_{\parallel,\perp}(t) - I_0}{\tau_D} \right), \tag{1}$$

where I_0 is the intensity of the equilibrium background fluorescence in the absence of photobleaching. I_0 is proportional to the incident input power, the absorption coefficient of the

dyes at the laser wavelength, and the dye concentration. The steady-state equilibrium value, once the balance between photobleaching and diffusion has been reached, will be given by

$$I_{\parallel,\perp}(t\rightarrow\infty)=I_0/(1+\tau_D/\tau_{\parallel}). \tag{2}$$

If $\tau_{\parallel,\perp}\ll\tau_D$ because I_0 is high, the decay time will be governed essentially by photobleaching and, according to Eq. (2), $I_{\parallel,\perp}(t\rightarrow\infty)\sim 0$. In this case, the measured decay times in $I_{\parallel}$ and $I_{\perp}$ will have the following properties [8]: $\tau_{\perp}>\tau_{\parallel}$ for $T<T_c$, $\tau_{\perp}=\tau_{\parallel}$ for $T>T_c$, $\tau_{\parallel,\perp}\propto I_0^{-2}$ at a fixed T, and $\tau_{\parallel}/\tau_{\perp}=\langle\sin^4(\Theta)\rangle_T/\langle\cos^4(\Theta)\rangle_T$ independent of I_0 for any T (T_c is the nematic-isotropic phase transition temperature). All these properties have been demonstrated in Ref. [8].

The diffusion time constant τ_D will also depend on temperature. Its temperature dependence is, however, more difficult to predict from a microscopic model than in the case of $\tau_{\parallel,\perp}$. It turns out that the diffusion process of a dye molecule within a LC can be reasonably well modeled by a temperature dependence of the form

$$\tau_D=\tau_D^0(1-e^{-T^*/T}), \tag{3}$$

where τ_D^0 is a constant and T^* is an activation temperature (energy). Equation (3) gives the appropriate limiting values of $\tau_D\rightarrow 0$ for $T\rightarrow\infty$ and $\tau_D\rightarrow\tau_D^0$ for $T\rightarrow 0$, which imply fast and saturated diffusion, respectively. For intermediate temperatures, Eq. (3) gives a smooth decreasing function of T, which implies a faster diffusive response of the system for higher temperatures.

By gathering the aforementioned formulas, we shall expect a temperature dependence of the steady state fluorescence emission (2) of the forms

$$I_{\parallel}/I_0=1/[1+C(I_0)(1-e^{-T^*/T})\langle\cos^4(\Theta)\rangle_T] \tag{4}$$

and

$$I_{\perp}/I_0=1/[1+C(I_0)(1-e^{-T^*/T})\langle\sin^4(\Theta)\rangle_T], \tag{5}$$

where $C(I_0)$ is a constant for a fixed I_0. The thermal averages $\langle\ \rangle_T$ of the director orientations in Eqs. (4) and (5) can be modeled as in Ref. [8], i.e., by using the self-consistent mean-field Maier-Saupe theory of the nematic state. The calculation can be greatly simplified if an analytic approximation for the order parameter $S(T)$ is used [8]. In Sec. II C we shall show the experimental verification of Eqs. (4) and (5).

Another aspect of interest for the forthcoming discussion will be the case of pure diffusion without photobleaching. If the intensity of the pumping laser is extended and weak enough, then $\tau_{\parallel,\perp}\gg\tau_D$, and photobleaching can be safely neglected. Suppose that a region, where an inhomogeneous dye concentration exists, is uniformly illuminated by a pumping laser, and a fluorescent image is obtained which reveals the dye distribution. Let us further assume that the dye distribution is inhomogeneous in one direction (x), since this will be the relevant case for the study in capillars. Furthermore, we assume that the LC is not oriented and, accordingly, that there is an average diffusion constant in the otherwise anisotropic nematic state. If the initial fluorescence

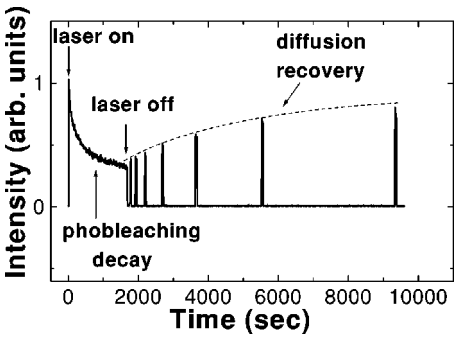

FIG. 2. Example of FPRS in a planar aligned LC cell of E_7 doped with DTDCI. The data have been taken for the $\parallel$ excitation. The laser is turned on initially with a power density of 2100 μW/mm^2, which implies that $\tau_{\parallel}\ll\tau_D$. Photobleaching dominates in the initial decay of the fluorescence. The excitation is subsequently turned off and diffusion replaces the photobleached molecules in the spot area. The laser is, a while later, reinstated several times for a few seconds to monitor the recovery of the fluorescence produced by diffusion. Note the square-root type of recovery of the signal. The dashed line following the diffusion recovery peaks is a guide to the eye. See text for further details.

has an intensity profile $I(x,t=0)$, the fluorescence for subsequent times will be given by

$$I(x,t)\propto\frac{1}{\sqrt{Dt}}\int_{-\infty}^{+\infty}I(x_0,0)e^{-(x-x_0)^2/4Dt}dx_0, \tag{6}$$

if a Gaussian (random walk) type of diffusion is assumed. In Eq. (6), $D=(D_{\parallel}+2D_{\perp})/3$ is an average diffusion constant for the dyes in the nematic state. By fitting the fluorescence intensity profiles for different times with an appropriate D, the average diffusion constant of the dyes within the LC can be accurately measured. It is worth noting at this point that diffusion in an oriented LC nematic film takes place in an anisotropic manner with two different diffusion constants $D_{\parallel}$ and $D_{\perp}$, akin to the self-diffusion process for the LC molecules themselves [12]. However, there is only one diffusion relaxation time τ_D affecting the magnitude of the fluorescence emission in Eqs. (1)–(5). This is easy to understand, since the contribution to the total fluorescence of a dye molecule moving into or out of the illuminated area cannot discern between parallel or perpendicular diffusion. In other words, once a molecule is within the laser spot, we cannot decide from its fluorescence emission whether the molecule came into that position from one direction or another. The anisotropy in the diffusive behavior of the molecules can be seen, nevertheless, by direct imaging of the evolution of photobleached molecules using the two-beam FPRS, as we shall show below. On the other hand, photobleaching does have two relaxation time constants $\tau_{\parallel,\perp}$, inasmuch as it is related to a direct coupling of the laser field with the molecule [8], and this can, of course, discern between a $\parallel$ or $\perp$ orientation.

In Sec. II C, we shall present the different experimental results, and make a connection to specific aspects of the models displayed here. Further details of the theoretical interpretation of the experiments will be given when appropriate.

C. FPRS and digital imaging

Figure 2 shows the prototype example of FPRS with one laser beam. In this case, an oriented dye doped nematic LC film is illuminated in parallel excitation with $HeNe_1$ in Fig. 1. The fluorescence emission at 695 nm is detected by the triple subtractive monochromator Mc coupled to the PMT. The emission is measured as a function of time at room temperature (23 °C) with a fixed input laser power density of 2100 $\mu W/mm^2$. This power density is high enough [8] for this excitation wavelength to assure that $\tau_{\parallel} \ll \tau_D$ and, as a consequence, the initial decay of the fluorescence emission will be essentially dominated by photobleaching. After 1800 sec the laser is turned off, whereupon diffusion takes over and starts replacing the photobleached region with new dye molecules. The laser is subsequently turned on for a few seconds at different times to observe the recovery of the fluorescence with a minimum effect of photobleaching. As can clearly be seen in Fig. 2, the fluorescence recovers steadily after the laser has been turned off and, for this particular LC (E_7) and dye (DTDCI) it takes about 2 h to recover the initial fluorescence in the illuminated area. The data in Fig. 2 are the archetype examples of FPRS and, in fact, the photobleaching and diffusion time constants can be directly measured from here. Note also that the fluorescence recovers with square root type of law (dashed line in Fig. 2), in accordance with a Gaussian-like diffusion.

Conversely, there are other aspects of the diffusion process which cannot be observed by FPRS as presented in Fig. 2. The anisotropy of the diffusion, for instance, cannot be directly acquired from a one-beam FPRS experiment. This is where the two-beam FPRS technique comes into play. Let us assume now that we illuminate the sample with both $HeNe_1$ and $HeNe_2$ in Fig. 1. The beam from $HeNe_2$ ($\vec{E}_L^2$) is expanded to reduce the power density, and it is polarized $\perp$ to $\vec{n}$ to minimize its photobleaching effect. The beam also covers a wide area so that it monitors the dye concentration, producing a *background* fluorescence. Accordingly, we call $HeNe_2$ a *probe beam*. $HeNe_1$, conversely, is focused to a small spot within the area covered by $HeNe_2$, and with its polarization $\parallel$ to $\vec{n}$. In addition, the power density of $HeNe_1$ is much higher than that produced by $HeNe_2$ in the same region. Thus the photobleaching rate at the spot of $HeNe_1$ will be much faster than the one produced by the probe beam. If $HeNe_1$ is left for a few seconds and then turned off, there will be a region within the illuminated area of $HeNe_2$ where the dyes exhibit less fluorescence. In other words, it is possible to *dig a hole* in the background fluorescence of $HeNe_2$ by the faster photobleaching effect of $HeNe_1$. This is shown in Fig. 3 over a wide area where the full illumination produced by $HeNe_2$ can be seen. In Fig. 3(a), the Gaussian-like intensity profile of the expanded probe beam can be easily observed. In Fig. 3(b), $HeNe_1$ has been turned on for a few seconds at the position labeled as the *laser spot*. Finally, Fig. 3(c) shows the smearing of the photobleached region a few minutes later. The digital images in Fig. 3 have been obtained with Mc in a double subtractive configuration with an intermediate slit of ~ 5 mm assuring a spectral width of 2 nm around 695 nm in the filtered image that reaches the CCD camera. Normally, the study of the details of the diffusion process requires a much tighter focused laser spot from

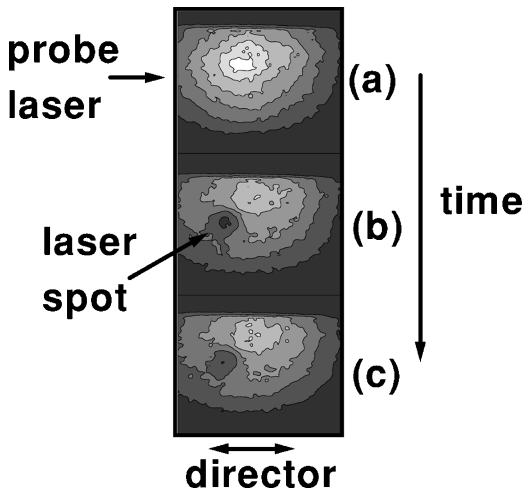

FIG. 3. General view of two-beam FPRS spectroscopy in a planar aligned LC cell of E_7 doped with DTDCI. Darker colors imply fewer fluorescence emissions. The digital images represent the fluorescence at 695 nm of the resonantly pumped DTDCI molecules at room temperature. In (a), only the probe expanded beam from $HeNe_2$ is shown with its characteristic Gaussian profile. The beam has approximately 10 mm in diameter. $HeNe_1$ is focused in the region labeled as laser spot with a diameter of ~ 1 mm, and is turned on for a few seconds. The clear contrast between the photobleached area by $HeNe_1$ and the background fluorescence of $HeNe_2$, as well as its time evolution, can be clearly seen in (b) and (c). The images in (b) and (c) have been taken at 10 and 20 min after $HeNe_1$ has been turned off.

$HeNe_1$ than the one shown in Fig. 3. In fact, in order to evaluate the details of the diffusion process, it is far better to have a nearly homogeneous fluorescence background from the probe beam, and this can be achieved by observing the effect of $HeNe_1$ over a very small area where the Gaussian profile of $HeNe_2$ can be ignored. Likewise, the observation of anisotropic diffusion is better observed if a long enough time is allowed for the initial perturbation to develop. However, the longer the time the poorer the contrast of the photobleached spot with respect to the fluorescence background of the probe. In addition, the inevitable imperfections of the sample (like inhomogeneities or small domains with slightly different orientations) become more evident for longer times. Accordingly, the observation of the diffusion dynamics by the two-beam FPRS method requires a compromise between laser spot size, intensity, and elapsed time for diffusion.

Figure 4 shows images from a two-beam FPRS experiment over a smaller area of the LC cell. The light greyish area in Fig. 4(a) displays, actually, a small region within one of the rings in Fig. 3(a). $HeNe_1$ is focused down to a spot of 0.25 mm in diameter, and it is turned on for 10 sec. Figures 4(b), 4(c), and 4(d) show the time evolution of the photobleached region at 10, 20, and 40 min after $HeNe_1$ has been turned off. It is quite clear from Fig. 4 that (i) the perturbation produced by $HeNe_1$ in the background fluorescence of $HeNe_2$ becomes elliptic due to the anisotropy of the diffusion coefficients; (ii) contrast is being lost as a function of time because the fixed number of photobleached molecules created by $HeNe_1$ spread, and their density per unit volume is decreased; and (iii) imperfections in the diffusion pattern of the photobleached region become evident after 40

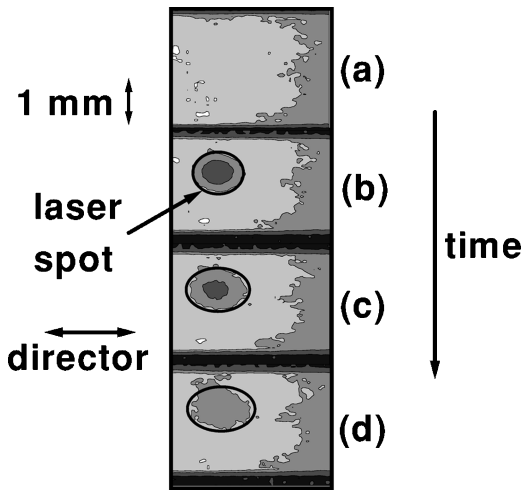

FIG. 4. Same as Fig. 3 for a smaller area within the probe beam. $HeNe_1$ is focused down to a spot of 0.25 mm in this case, and the time evolution of the photobleached region is monitored after 10, 20, and 40 min. The thick black line encircling the spot is a guide to the eye. Note the increasing anisotropy in the shape of the spot, the loss of contrast, and the appearance of imperfections around the boundary for $t=40$ min. The diffusion constant of the photobleached molecules is slightly larger along the director orientation of the planar aligned LC cell. See the text for further comments.

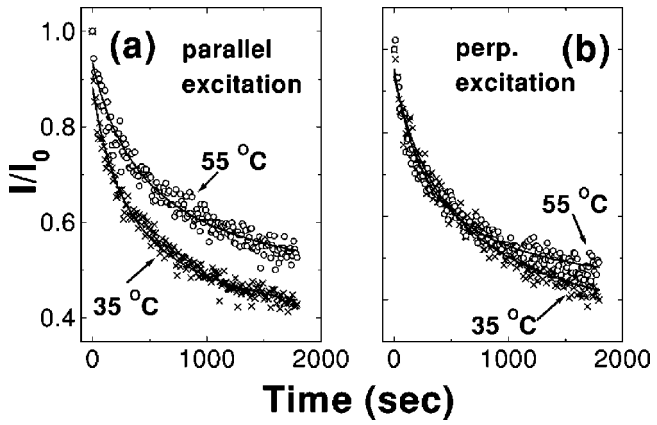

FIG. 5. Fluorescence decays at two different temperatures $T=35$ and 55 °C (below $T_c=63$ °C) for the $\parallel$ (a) and $\perp$ (b) excitation conditions. Note that $I_{\parallel}(55\,°C)$ decays more slowly than $I_{\parallel}(35\,°C)$ in (a), while the opposite occurs in (b). On the other hand, the signal at 55 °C is larger than the one at 35 °C in both cases, if a sufficiently long time passes. The data have been taken at 695 nm with a triple subtractive configuration of M_c and the PMT. The incident laser power density from $HeNe_1$ was 630 $\mu W/mm^2$ and, accordingly, the initial decay time is influenced by both photobleaching and diffusion.

min, mainly in the periphery of the spot. Figure 4 shows explicitly how the diffusion process can be directly studied in an anisotropic fluid like an oriented LC. It can, in fact, render the anisotropy of the diffusion coefficients, which is normally very difficult to measure accurately for a small concentration of molecules within a solvent fluid. In order to obtain a numerical estimate for the anisotropy, it is necessary to model the diffusion process. By assuming a two-dimensional (2D) Gaussian diffusion model triggered by a uniform circular photobleached region with the size of the laser spot, it is possible to fit the fluorescence images in Fig. 4. From best fits of images (b), (c), and (d) in Fig. 4, we obtain the anisotropy to be $D_{\parallel}/D_{\perp}\sim 0.82\pm 0.08$, somewhat larger compared to the anisotropies found in self-diffusion coefficients in LC's. Note, however, that $D_{\parallel}>D_{\perp}$, exactly as in the self-diffusion of LC's. This latter property is, actually, most likely to have a microscopic explanation in the elongated molecular shape of dye and LC molecules than in the details of the molecular interactions among them. Not only the anisotropy but also the absolute value of the diffusion coefficients can also be obtained from the fit within 10–15 %. This is not however the most accurate method for their determination. In general, it is more convenient to measure the pattern of a diffusing substance over a long period of time to be able, in that manner, to measure the spread over larger distances and reduce the relative error. Notwithstanding, due to the loss in contrast in the digital imaging of the photobleached region, a relatively large error is introduced in the evaluation of the form and size of the photobleached area after a long period of time has run by. As we shall show below, a better quantitative measurement of the diffusion coefficient can be obtained from a situation in which $\tau_{\parallel,\perp}>\tau_D$ in the capillary tubes.

One important question to address at this moment is the difference between the diffusion of a dye molecule and a photobleached dye molecule. On a microscopic level, photobleaching occurs in cyanines like DTDCI ($C_{23}H_{23}N_2S_2:I^-$) by dissociation of the *added* I^- atom from the central backbone of the molecule. This is supported by quantum chemical calculations of the total energy and the reaction path coordinates [13] by means of a semiempirical Hamiltonian like the Austin model 1 [14]. The most important general structural features of the backbone of the molecule, however, remain unaltered. Moreover, there is no direct chemical interaction with the LC host, either before or after photobleaching. We can, therefore, safely assume that diffusion of photobleached molecules is, to a very good approximation, identical to that of unbleached molecules. The evolution of the *photobleached cloud* of dyes in Figs. 3 and 4 is, accordingly, representative of the dyes themselves.

Further insight into the dye diffusion dynamics within an oriented nematic LC cell can be obtained by direct measurement of the fluorescence decay in parallel or perpendicular excitation as a function of temperature. According to the models introduced in Sec. II B we expect τ_D to decrease when T is raised and, after a sufficiently long time, $I_{\parallel,\perp}(T_2)/I_0>I_{\parallel,\perp}(T_1)/I_0$ if $T_1<T_2$. Moreover, we expect $\tau_{\parallel}(T)$ to increase with temperature since $\langle\cos^4(\Theta)\rangle_{T_2}<\langle\cos^4(\Theta)\rangle_{T_1}$ if $T_1<T_2<T_c$ in the nematic state [8]. Conversely, $\tau_{\perp}(T_2)<\tau_{\perp}(T_1)$, because $\langle\sin^4(\Theta)\rangle_{T_2}>\langle\sin^4(\Theta)\rangle_{T_1}$. As a consequence, upon raising the temperature from T_1 to T_2, we expect the fluorescence for the $\parallel$ excitation condition to show a slower decay and to have a limiting value for sufficiently long times which is above that of T_1. This implies, as a consequence, that $I_{\parallel}(T_2)>I_{\parallel}(T_1)$ for all times. For the $\perp$ excitation, however, we expect $I_{\perp}(T_2)$ to initially decay faster [$I_{\perp}(T_2)<I_{\perp}(T_1)$ for $t\sim 0$] but, since $I_{\perp}(T_2)/I_0>I_{\perp}(T_1)/I_0$ for $t\to\infty$, there must be a crossover to reassure this condition. This is clearly seen in Figs. 5(a) and 5(b), where the fluorescence from the parallel and perpendicular excitation conditions are compared for two different tem-

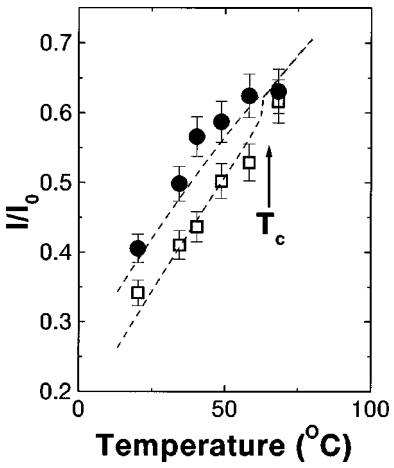

FIG. 6. $I_{\parallel}(t\rightarrow\infty)/I_0$ (open squares) and $I_{\perp}(\rightarrow\infty)/I_0$ (closed circles) as a function of T. The data have been obtained from the exponential decay fits of the fluorescence signal over a period of time of 1800 sec at 695 nm with the $HeNe_1$ excitation (see Fig. 1) in $\parallel$ or $\perp$ excitation, and a power density of 630 μW/mm^2. The dashed lines are a (simultaneous) fit of both data sets with the model equations (4) and (5). The average increase of I/I_0 is due to the rise in dye diffusion, while the difference between the two curves is accounted for by the distinct photobleaching time constants $\tau_{\parallel,\perp}$. The difference vanishes above $T_c\sim 63\,^{\circ}$C, as expected.

peratures below T_c. The solid lines in Fig. 5 are best fits to the data with exponential decays. In Fig. 5(a), the data for $T=55\,^{\circ}$C display a slower decay and the limiting value of the fluorescence for sufficiently long times is above the signal at 35 °C. Conversely, the $\perp$ excitation condition in Fig. 5(b) shows a faster fluorescence decay for $T=55\,^{\circ}$C with a crossover producing $I_{\perp}(55\,^{\circ}\mathrm{C})>I_{\perp}(35\,^{\circ}\mathrm{C})$ for sufficiently long times, as predicted by the model. In addition, from these very same fits to the data we can plot the values of $I_{\parallel,\perp}(t\rightarrow\infty)/I_0$ for different temperatures, and compare them with the predictions of Eqs. (4) and (5) in Sec. II B. This is done in Fig. 6, where the values have been obtained for several temperatures below (and one slightly above) T_c. The dashed lines in Fig. 6 are a fit with Eqs. (4) and (5). The thermal orientational averages $\langle\sin^4(\Theta)\rangle_T$ and $\langle\cos^4(\Theta)\rangle_T$ have been obtained with the self-consistent mean-field Maier-Saupe theory, with an analytic approximation for the order parameter of the nematic state, as in Ref. [8]. Note that for a given set of parameters $C(I_0)$ and T^* in Eqs. (4) and (5) the two curves in Fig. 6 are fit together, i.e., the dashed lines in Fig. 6 represent a simultaneous fit of two curves with two free parameters. The physical meaning of the data in Fig. 6 is quite clear in light of the interpretation given in Sec. II B. Both $I_{\parallel}(t\rightarrow\infty)/I_0$ and $I_{\perp}(t\rightarrow\infty)/I_0$ increase with temperature because the average diffusion of the dyes increases when T is raised. However, the input laser discerns between $I_{\parallel}$ and $I_{\perp}$ on account of the polarization dependence of the photobleaching decay rates $\tau_{\parallel,\perp}$. In this manner, the two curves in Fig. 6 are a compromise between the increasing mobility of the dyes and the anisotropic coupling to the laser polarization guided by the order parameter of the LC. The difference between the two vanishes above T_c, as expected from an isotropic phase.

To complete the experimental results, in Sec. II D we shall show another form of spectroscopic experiment which

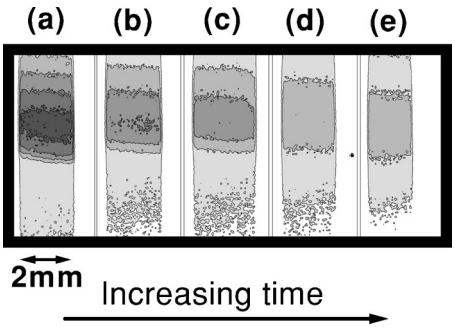

FIG. 7. Dye diffusion through a thick (~ 7 mm) capillar. Only the fluorescence at 695 nm of the central part (~ 2 mm) of the capillar is imaged. At $t=0$ the capillar is half-filled [bottom half in (a)] with pure E_7, and the upper half is filled with a mixture of E_7 and DTDCI. The initial concentration in (a) (darker colors represent higher concentrations) is clearly seen to spread as a function of time. The images have been taken at $t=0$, 30, 60, 450, and 1140 min.

can be carried out in the opposite limit where $\tau_{\parallel,\perp}\gg\tau_D$ and, accordingly, the presence of photobleaching can be neglected. Further comparison with the aforesaid models is also conferred.

D. Diffusive regime

The limit $\tau_{\parallel,\perp}\gg\tau_D$ implies that the total effective decay time [8] $1/\tau_{\mathrm{eff}}=1/\tau_D+1/\tau_{\parallel,\perp}$ is completely dominated by diffusion. This situation is experimentally realized when the incident laser is expanded to a large area in order to monitor the evolution of a dyed region and, in this manner, the incident power density is considerably smaller and the diffusive replacement of photobleached molecules is much faster than $\tau_{\parallel,\perp}$. As a matter of fact, we could always use this situation to monitor the diffusion of dyes (or tagged molecules) without having the additional ingredient of photobleaching. However, it is very helpful to have a small region with a well controlled initial geometry for the dyes to start observing the diffusion process, and this is frequently much more laborious in the present case. If we observe the diffusion of photobleached dyes in a homogeneous background of unbleached molecules, we define the initial conditions with the external optics. As in the case of two-photon scanning microscopy with FPRS [4], the initial geometrical distribution of photobleached molecules can be controlled very accurately, and this, without doubt, facilitates the subsequent interpretation of the data. Needless to say, this is particularly crucial in cases where anisotropies or inhomogeneities are present. If we study a case where $\tau_{\parallel,\perp}\gg\tau_D$, conversely, the initial dye distribution is given, or must be produced, by *mechanical* means. A small well defined volume can only be obtained by *injecting* the dyes or tagged molecules within the sample. This is normally very difficult if we wish to study, for instance, dye diffusion within a LC cell which may have only a thickness of ~ 10–100 μm. In this sense, the two situations depicted in this and the previous subsections represent two aspects of the same problem, and, undoubtedly, both have advantages and weaknesses.

In Fig. 7 we explicitly show an example of dye diffusion through a thick capillar filled with an unoriented nematic LC and $\tau_{\parallel,\perp}\gg\tau_D$. The thick quartz capillar with a diameter of

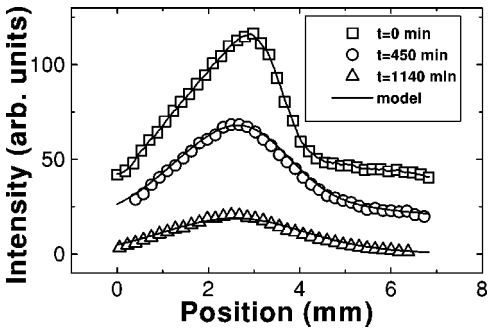

FIG. 8. Dye concentration profiles along the diffusion direction taken from the images in Fig. 7. By defining the curve at $t=0$ as $I(x_0,0)$, the solid lines for $t=450$ and 1140 min are a fit with Eq. (6), and $D=1.02\times10^{-7}$ cm^2 sec^{-1}. The curves have been vertically shifted for display purposes. Further details are given in the text.

$d\sim5$ mm is half-filled with unoriented and undoped E_7 at room temperature. The sample is illuminated from the back with the expanded beam from $HeNe_2$ in order to obtain a fairly homogeneous illumination at the observation point. The beam is expanded twice in this case to assure this condition. At $t=0$, the upper half of the capillar is filled with a mixture of E_7 and DTDCI (10^{-2} mg/ml), and the filtered image at 695 nm of the central part of the capillar (to avoid considering the effect of the walls) is observed with the CCD array and Mc in double subtractive configuration. An integration time of 10 sec has been used for these images. In Fig. 7, the initial inhomogeneous dye concentration is clearly seen to spread by diffusion as a function of time. By virtue of the geometry and constraints, this is a typical example which can be adequately well described by a 1D diffusion problem. By averaging the concentration profiles in Fig. 7 perpendicular to the diffusion direction, we obtain the curves in Fig. 8 for three representative times. If the initial concentration profile at $t=0$ is defined as $I(x_0,0)$, the succeeding profiles can be easily predicted from Eq. (6) if an adequate value of D is chosen. This is explicitly shown in Fig. 8 for $t=450$ and 1140 min, where the solid lines are the predictions of Eq. (6) using the concentration profile for $t=0$ as $I(x_0,t)$ and $D=1.02\times10^{-7}$ cm^2 sec^{-1}. It is worth noting that, for the molecular weight of the dyes under consideration, gravity has no measurable effect on the diffusion profile. As can easily be seen from Fig. 8, the Gaussian diffusion model in Eq. (6) can successfully account for the spread in the initial dye concentration profile. Furthermore, diffusion takes place in this case through an unoriented LC and, accordingly, D represents the average diffusion constant $D=(D_\parallel+2D_\perp)/3$ of the dyes. Situations in which the LC is oriented within the capillar by proper surface treatment and/or the temperature is varied are obviously possible. Moreover, loss of contrast in the concentration profile is only achieved at extremely long times in comparison with the photobleaching method, as the number of observed molecules is much larger than the typical number of photobleached molecules achieved after a few seconds of illumination with $HeNe_1$. This results in a more accurate value of the diffusion coefficient. Combining the diffusion anisotropy observed with photobleaching in Sec. II C, and the average diffusion D obtained here, we deduce $D_\parallel=7.92\times10^{-8}$ cm^2 sec^{-1} and $D_\perp=7.37\times10^{-8}$ cm^2 sec^{-1} at room temperature. In Sec. III, we shall summarize the principal features of the experiments reported in this subsection and Sec. II C as well as their interpretation, and, in addition, the plausible usage of Raman rather than fluorescence spectroscopy to image diffusion processes will be discussed.

III. DISCUSSION AND CONCLUSIONS

Throughout this paper we showed the interplay between diffusion and photobleaching in a prototype dye doped nematic LC through (i) the application of FPRS with one or two laser beams, (ii) digital imaging of the fluorescence emission, and (iii) the effect of temperature and/or the intrinsic order of the LC. To the very best of our knowledge, this is the first study by pure optical means where the diffusion process of dyes within a LC is directly studied and imaged. Diffusion in an *anisotropic fluid* like a LC is not at all very common and the combination of one- or two-beam FPRS with digital imaging opens the possibility to study several aspects of the diffusion dynamics. While the one-beam FPRS technique allows a direct measurement of the interplay between photobleaching and diffusion, the involved time constants, and the effect of temperature (Figs. 2, 5, and 6), the microscopic observation of the diffusion anisotropy as well as the regime $\tau_{\parallel,\perp}\gg\tau_D$ are better observed by either two-beam FPRS or direct digital imaging with a uniform illumination (Figs. 3, 4, and 7). As pointed out above, all these experiments indeed represent different faces of the same problem. Diffusion and photobleaching are two important physical properties of dye doped LC's which are relevant not only for the prediction of tailor made electro-optic devices [11], but also for the understanding of other experiments like transient thermal gratings generated by dye absorption [9], photothermal self-phase modulation [15], or transient and permanent optical recording [10]. In this latter experiments, the diffusion time constant of the dyes as compared to the repetition rate of the laser play a central role in the steady-state characteristics of the induced thermal modulation affecting the laser. Thermal gratings produced by dye absorption are sometimes induced in LC's to study more complicated situations which arise by further application of external electric or magnetic fields [9]. A basic understanding of diffusion and photobleaching in the most simple cases is, in this sense, important.

It is quite interesting to note that direct digital imaging with the spectral filtering of the double subtractive configuration in the monochromator is, by no means, restricted to the observation of fluorescence. Actually, Raman signals can also be imaged by this method, and provide a much more specific signature of a substance under study than fluorescence. Raman signals are, notwithstanding, much weaker, and normally require a better illumination from the laser. They have the benefit, however, that they are intrinsic of a substance which may not display fluorescence for the particular laser under use. Conventional Raman imaging is obtained as in Fig. 9(a). A laser spot with a given resolution is scanned through the region of interest, and the intensity of a Raman peak is monitored as a function of position. The spectra in Fig. 9(a) have been taken with Mc in a triple subtractive configuration with the CCD observing the dispersion of

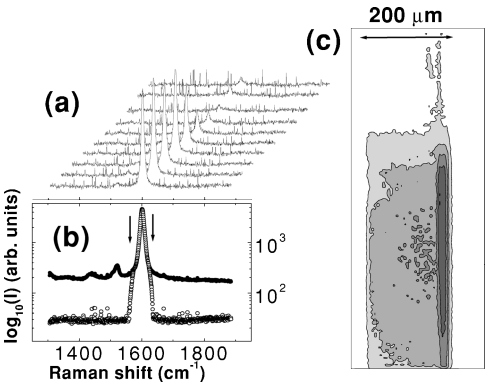

FIG. 9. (a) Raman imaging through a 1D scan. The $\sim$1600 cm^{-1} Raman mode of E_7 is monitored as a function of position. The different data are a scan of ten positions separated by 10 μm along a line crossing the interface of the LC. The decrease in intensity indicates the interface of the LC. (b) Effect of the intermediate slit of Mc in the double subtractive configuration. Note that the intensity is on a logarithmic scale. The intermediate slit can isolate the signal coming from the Raman mode of interest for the subsequent 2D imaging. (c) 2D Raman image of a 200-μm-thick capillar partly filled with E_7 taken with 10-sec integration time. A gliding trail of LC adhered to the capillar wall can also be seen.

the third grating. Conventional Raman imaging is composed of hundreds of spectra like these, which have to be combined to give a map of intensity vs position. A 2D scan is necessary to render an image, and there is the additional possibility of working with the depth of focus if the imaging is made confocal. An alternative to this is direct 2D imaging with the double subtractive configuration and a homogeneous laser illumination. The homogeneity of the illumination is achieved by overfilling a microscope objective with an inverted telescope [13]. In Fig. 9(b) we show the result of isolating the Raman peak under study with the intermediate slit of the double subtractive Mc. Note that the scale in Fig. 9(b) is logarithmic. It is possible to have an almost perfect rejection of unwanted signals forming the filtered image. Figure 9(c) shows a Raman image of a 200-μ-m thick capillar filled with E_7. The image takes 10 sec of integration time with an input power of 200 mW at the 514.5-nm line of an Ar^+-ion laser. It is quite clear that this technique allows the study of diffusion phenomena in a way that the 1D composition of spectra can never achieve. One of the main problems in the 1D scanning is that there is considerable delay between the signal coming from different regions of the sample due to integration and/or scanning time. These problems are essentially avoided in the present method, and results of interdiffusion of transparent nematogens and/or biologically relevant liquids will be published elsewhere [13].

ACKNOWLEDGMENTS

Special thanks are due to F. Tutzauer, R. Gludovats, C. Eggenschwiler, R. Soto, and B. Eckardt for technical help. It is a pleasure to thank M. Nöllmann and D. Shalóm, who provided some of the original ideas to perform the experiments reported in this work. A. Fainstein and Willy Pregliasco are gratefully acknowledged for stimulating discussions and general support. The author thanks the Fundación Antorchas for financial support through a reentry grant.

[1] X. H. Xu and E. S. Yeung, Science **275**, 1106 (1997).
[2] N. B. Cole, C. L. Smith, N. Sciaky, M. Terasaki, M. Edidin, and J. Lippincott-Schwartz, Science **273**, 797 (1996), and references therein.
[3] C. Sybesma, *An Introduction to Biophysics* (Academic, London, 1977), p. 35.
[4] J. Manni, Biophotonics **3** (1), 44 (1996).
[5] M. J. Stephen and J. P. Straley, Rev. Mod. Phys. **46**, 617 (1974); P. G. deGennes, *The Physics of Liquid Crystals* (Clarendon, Oxford, 1974); S. Chandrasekhar, *Liquid Crystals* (Cambridge University Press, New Rochelle, NY, 1980).
[6] G. H. Heilmeier, J. A. Castellano, and L. A. Zanoni, in *Proceedings of the International Liquid Crystal Conference* (Gordon, New York, 1968) Vol. 2-2, p. 763.
[7] I. Jánossy and L. Csillag, Phys. Rev. A **44**, 8410 (1991); I. Jánossy, Phys. Rev. E **49**, 2957 (1994); I. Jánossy, in *Proceedings of the NATO Advanced Research Workshop*, edited by F. Kajzar, V. M. Agranovich, and C. Y. C. Lee (Kluwer, Dordrecht, 1996), p. 477; I. Jánossy and T. Kosa, Opt. Lett. **17**, 1183 (1992).
[8] M. Nöllmann, D. Shalóm, P. Etchegoin, and J. Sereni, previous paper, Phys. Rev. E **59**, 1850 (1999).
[9] I. C. Khoo, H. Li, and Yu Liang, IEEE J. Quantum Electron. **QE-29**, 1444 (1993); H. Li, Yu Liang, and I. C. Khoo, Mol. Cryst. Liq. Cryst. **251**, 85 (1994); I. C. Khoo, *Liquid Crystals, Physical Properties and Nonlinear Optical Phenomena* (Wiley Interscience, New York, 1995).
[10] W. M. Gibbons, P. J. Shannon, S. T. Sun, and B. Swetlin, Nature (London) **351**, 49 (1991).
[11] G. H. Heilmeier and L. A. Zanoni, Appl. Phys. Lett. **13**, 91 (1968); H. J. Coles, H. F. Gleeson, and J. S. Kang, Liq. Cryst. **5**, 1243 (1989).
[12] L. M. Blinov, *Electro-Optical and Magneto-Optical Properties of Liquid Crystals* (Wiley Interscience, Chichester, 1983).
[13] P. Etchegoin (unpublished).
[14] M. J. S. Dewar, E. G. Zoebisch, E. F. Healy, and J. J. P. Stewart, J. Am. Chem. Soc. **107**, 3902 (1985); see also related methods in M. J. S. Dewar and W. Thiel, *ibid.* **99**, 4899 (1977).
[15] H. Ono and N. Kawatsuki, Jpn. J. Appl. Phys., Part 2 **36**, L353 (1997); Appl. Phys. Lett. **70**, 2544 (1997).